RAA 2015 Vol. **15** No. **10**, 1713–1724 doi: 10.1088/1674–4527/15/10/008
http://www.raa-journal.org *http://www.iop.org/journals/raa*

Research in Astronomy and Astrophysics

MHD Seismology of a loop-like filament tube by observed kink waves

Vaibhav Pant[1], Abhishek K Srivastava[2], Dipankar Banerjee[1,3], Marcel Goossens[4], Peng-Fei Chen[5,6], Navin Chandra Joshi[7] and Yu-Hao Zhou[5,6]

[1] Indian Institute of Astrophysics, Bangalore-560 034, India; *vaibhav@iiap.res.in*
[2] Department of Physics, Indian Institute of Technology (BHU), Varanasi-221005, India
[3] Center of Excellence in Space Sciences, IISER Kolkata 741246, India
[4] Centre for Mathematical Plasma Astrophysics, Department of Mathematics, KU Leuven, Celestijnenlaan 200B, B-3001 Leuven, Belgium
[5] School of Astronomy and Space Science, Nanjing University, Nanjing 210093, China
[6] Key Lab of Modern Astronomy and Astrophysics, Nanjing University, Nanjing 210093, China
[7] School of Space Research, Kyung Hee University, Yongin, Gyeonggi-Do, 446-701, Korea

Received 2014 November 12; accepted 2015 March 6

Abstract We report and analyze observational evidence of global kink oscillations in a solar filament as observed in Hα by instruments administered by National Solar Observatory (*NSO*)/Global Oscillation Network Group (*GONG*). An M1.1-class flare in active region (AR) 11692 occurred on 2013 March 15 and induced a global kink mode in the filament lying towards the southwest of AR 11692. We find periods of about 61–67 minutes and damping times of 92–117 minutes at positions of three vertical slices chosen in and around the filament apex. We find that the waves are damped. From the observed period of the global kink mode and damping timescale using the theory of resonant absorption, we perform prominence seismology. We estimate a lower cut-off value for the inhomogeneity length scale to be around 0.34–0.44 times the radius of the filament cross-section.

Key words: Sun: oscillations — Sun: magnetic fields — Sun: filament

1 INTRODUCTION

Solar prominences manifest various kinds of magnetohydrodynamic (MHD) oscillatory motions (Arregui et al. 2012). These oscillations are broadly classified either as large amplitude oscillations where the prominence as a whole oscillates with a velocity amplitude of a few tens of km s^{-1} or as small amplitude oscillations localized in a part of the prominence with a velocity amplitude of about 2–3 km s^{-1}. Many cases of prominence thread oscillations with small amplitudes have also been reported (Yi et al. 1991; Yi & Engvold 1991). Horizontal flows with simultaneous transverse oscillations were described by Lin et al. (2003), Lin et al. (2005) and Okamoto et al. (2007). Okamoto et al. (2007) characterized the propagating Alfvén waves in the filament threads and calculated the wave velocity to be about 1050 km s^{-1}. However, later Terradas et al. (2008) correctly interpreted them as standing kink waves and calculated the lower bound of Alfvén velocity in these threads with a lower value of 120 km s^{-1}. Lin et al. (2009) also reported the existence of propagating kink waves

in filament threads. Ning et al. (2009) found vertical and horizontal oscillations in the prominence threads with simultaneous drifting in the plane of the sky.

There have been numerous reports on small amplitude oscillations and large amplitude oscillations that are summarized in review articles by Oliver & Ballester (2002) and Tripathi et al. (2009) respectively. Ramsey & Smith (1966) reported observational evidence of large amplitude oscillations induced by disturbances coming from a nearby flare. Recent observations of large amplitude oscillations were reported in Hα (Eto et al. 2002; Jing et al. 2003; Okamoto et al. 2004; Jing et al. 2006; Liu et al. 2013), in Extreme Ultraviolet (EUV) (Isobe & Tripathi 2006) and in He 10830 infrared emissions (Gilbert et al. 2008). The most recent report was by Hershaw et al. (2011) in which they investigated two damped large amplitude transverse oscillations in an EUV prominence on the solar limb. The large amplitude oscillations can be either longitudinal (Jing et al. 2003, 2006; Vršnak et al. 2007; Li & Zhang 2012; Luna & Karpen 2012; Luna et al. 2012; Zhang et al. 2012; Luna et al. 2014) or transverse (Isobe & Tripathi 2006; Okamoto et al. 2004; Schmieder et al. 2013). Detection of MHD waves and oscillations provides important input in diagnosing the local plasma conditions of the solar corona by applying the principle of MHD seismology (Nakariakov & Verwichte 2005; Andries et al. 2005, 2009; Ruderman & Erdélyi 2009). The fundamental mode of the global kink wave is characterized by a displacement of the magnetic flux tube where all its parts are in phase (Nakariakov et al. 1999). In the MHD regime, the global transverse oscillations of magnetic flux tubes are interpreted as nearly incompressible fast kink modes (Edwin & Roberts 1983; Roberts et al. 1984; Erdélyi & Taroyan 2008; Van Doorsselaere et al. 2008; Goossens et al. 2009).

Prominence oscillations are often found to be damped (Ruderman & Roberts 2002; Erdélyi & Taroyan 2008; Andries et al. 2009; Arregui & Ballester 2011). Damping is observed in both large amplitude oscillations where the prominence oscillates as a whole (Hershaw et al. 2011) and at smaller scales, where different parts of the prominence show different damping timescales (Terradas et al. 2002; Lin et al. 2009).

Besides the oscillation period, the damping timescale also provides fundamental information about the physical conditions around the prominence. The MHD seismology of the localized plasma environment of the magnetic flux tubes based on both the oscillation period and damping timescale of transverse waves is performed in a consistent manner by Goossens et al. (2006); Arregui et al. (2007); Goossens (2008); Goossens et al. (2008); Soler et al. (2013). These fast kink radial modes get attenuated, probably due to the resonant absorption, and are converted into dominantly torsional (azimuthal) highly incompressible motion (Ruderman & Roberts 2002; Goossens et al. 2002, 2006, 2008, 2013; Goossens 2008; Arregui et al. 2008). However, other mechanisms (e.g., dissipation through wave leakage, curvature effects, phase mixing, etc.) can also be at work in dissipating such waves in the solar coronal tubes (e.g, Ruderman & Roberts 2002; Ofman & Wang 2002; Srivastava et al. 2013).

In this paper, we present evidence of large amplitude, long period damped transverse oscillations in a solar filament as observed by instruments that are administered by National Solar Observatory (*NSO*)/Global Oscillation Network Group (*GONG*) in Hα. We interpret them as global kink waves as they displace the prominence tube as a whole in the transverse mode. Such an analysis has been carried out by Hershaw et al. (2011), but they have reported the kink oscillations in EUV and there were differences in the periods of the two legs of the prominence. With that, the two legs of the prominence initially oscillated in phase and then gradually moved out of phase. Okamoto et al. (2004) and Eto et al. (2002) observed winking filaments in Hα with intermediate periods (20–40 min). However, there was no signature of damping. Isobe & Tripathi (2006) and Chen et al. (2008) also reported undamped transverse oscillations, which happened during or immediately prior to eruption. Gilbert et al. (2008) described long period, large amplitude vertical oscillations but the damping time observed by them was six times the period of oscillation. Prominence seismology in large amplitude oscillations has been carried out by Pintér et al. (2008) and Vršnak et al. (2007), and in prominence threads by Lin et al. (2009). This paper is organized as follows: In Section 2, we briefly present

the observations. We describe the detection of kink oscillations in Section 3. In Section 4, we perform the MHD seismology and estimate the localized physical conditions within the filament. In Section 5, the discussions and conclusions are outlined.

2 OBSERVATIONS

An M1.1-class flare was observed by the *GOES* satellite in the active region AR 11692 on 2013 March 15, which was associated with a halo coronal mass ejection (CME). Soon after the onset of the flare, oscillations were observed in the filament lying southwest of the active region as seen in Hα from *NSO*/*GONG* (Fig. 1, right panel, the movie is available on *http://www.raa-journal.org/docs/Supp/ms2083.mpeg*).

Instruments administered by *NSO*/*GONG* provide full-disk observations of the Sun at 6563 Å. These have a maximum pixel resolution of $\sim$1.07$''$ and a cadence of 1 minute. The flare or the associated CME generated global disturbances that in turn triggered the observed transverse oscillations in the body of the filament. Observations started at 06:00:54 UT and ended at 10:22:54 UT. At least four transversal cycles of the global transverse oscillations are observed with their significant damping. The left panel of Figure 1 shows the Helioseismic and Magnetic Imager (HMI) magnetogram contours overlayed on the image observed by Atmospheric Imaging Assembly (AIA) on board *Solar Dynamics Observatory* (*SDO*) at 304 Å. AIA observes the Sun in seven EUV bandpasses and has a pixel size of 0.6$''$(Lemen et al. 2012). The 304 Å images are chosen because in this passband the footpoints of the filament can be identified. Footpoints are identified by examining the strands of the filament in the image together with contours outlining regions with opposite polarities because a filament always lies on the polarity inversion line. Footpoints are marked as 'X' (negative) and 'Y' (positive) on the image. Green and black contours represent constant magnetic field strength of 20 G and –20 G, respectively. We chose five points over the filament between the footpoints 'X' and 'Y'. We then interpolate the curve using a cubic spline between the footpoints. The interpolated curve has to pass through the five chosen points. The length of the interpolated curve should be approximately equal to the length of the filament. We repeat this process several times by choosing five different points every time between 'X' and 'Y'. Therefore, the length of the interpolated curve will vary, and its mean value and standard deviation can be estimated. The length of the filament, L, is measured to be $\sim 235\pm8$ Mm.

3 DETECTION OF GLOBAL KINK OSCILLATIONS IN A FILAMENT TUBE

The evolution of the oscillations is tracked by placing three artificial slices close to the apex of the filament parallel to the observed oscillations and perpendicular to the filament (see the right panel of Fig. 1) using the Hα image sequence acquired by *NSO*/*GONG*. For each slice, a two dimensional time-distance diagram is created (see the left panels of Fig. 2), where the x-axis represents the time in minutes and the y-axis represents the distance along the slice in Mm. The thick black region represents the data gap from 07:07:54 UT to 07:18:54 UT. Along each column of the time-distance diagram, a Gaussian curve is fitted and the mean values with one-sigma error bars are estimated. The entire time-distance diagram is then fitted with a damped harmonic curve represented by the formula (Aschwanden et al. 1999)

$$y(t) = c + a_0 \sin(\omega t + \phi) e^{-t/\tau_{\rm d}}\,, \tag{1}$$

where c is a constant, a_0 is the amplitude, $\tau_{\rm d}$ is the damping time, ω is the angular frequency and ϕ is the initial phase.

The least squares fitting is performed using the function MPFIT.pro (Markwardt 2009) in Interactive Data Language (IDL). The best-fit curves are shown in Figure 2 (right panels). The period of the oscillation $P = \frac{2\pi}{\omega}$, the damping time $\tau_{\rm d}$ and the initial phase ϕ for the first (second and third) slices are found to be 67$\pm$3 min (63$\pm$2 min and 61$\pm$2 min), 98$\pm$47 min (117$\pm$45 min and

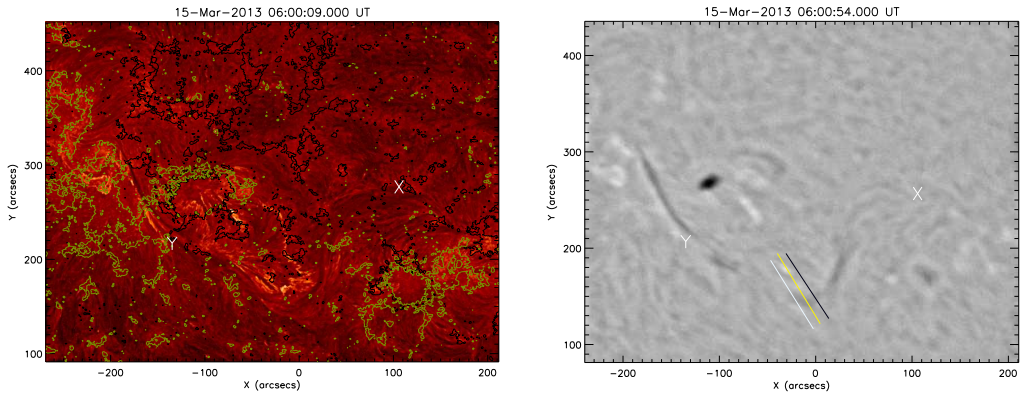

Fig. 1 The left panel shows the HMI magnetogram contours overlayed on the image as observed by AIA on board SDO at the 304 Å channel. The right panel shows the *NSO*/*GONG* Hα image of the filament southwest of AR 11692. The slices used for creating the time-distance map are marked as white, yellow and black slanted lines.

92±28 min) and 2.7±0.4 (2.9±0.3 and 2.7±0.3), respectively. From Figure 2 (right panels) we note that the filament segments at the three slices are oscillating in phase. The amplitude of the oscillation, a_0, is 8±4 Mm (9±3 Mm and 13±3 Mm) and the velocity amplitude is about 12±6 km s^{-1} (15±6 km s^{-1} and 22±7 km s^{-1}) for the first (second and third) slice, respectively. Oscillations with decaying amplitudes are also noticed near the footpoints of the filament. They are in phase with the oscillations seen near the apex of the filament. The in-phase displacement of the filament is interpreted as the global standing kink mode. Since all parts of the filament oscillate in phase and the footpoints of the filament are fixed, we infer it to be the fundamental standing mode. Moreover, it should be noted that we cannot distinguish, based on these observations, whether the oscillations are vertical or horizontal, or mixed. However, this does not affect the principle of the MHD seismology on the filament that we intend to implement in this study. Assuming the filament to be a flux tube embedded in a uniform magnetic field, the phase speed for the fundamental standing mode can be calculated using the relation,

$$v_{\rm ph} = \frac{2L}{P}\,. \tag{2}$$

As a result, $v_{\rm ph}$ for the first (second and third) slice is computed to be 117±9 km s^{-1} (124±8 km s^{-1} and 128±9 km s^{-1}), respectively. The sound speed, $c_{\rm s}$, with the chromospheric temperature is 15 km s^{-1}. With $v_{\rm ph} > c_{\rm s}$, we infer it to be a fast kink oscillation.

Prominence models in general invoke the fine structure of isolated/groups of prominence threads on which the MHD wave mode(s) is distributed (Arregui & Ballester 2011). In the present case, the almost bipolar prominence, having a rather small aspect ratio like the EUV loops, is subjected to the transverse displacement of its axis as a whole. Therefore, we treat it as a loop-like prominence tube supporting the kink oscillations.

4 CORONAL SEISMOLOGY OF THE OSCILLATING FILAMENT TUBE

We assume the filament to be a flux tube with its radius much smaller than its length, L (i.e., thin-tube approximation). With the thin tube approximation or long wavelength limit (i.e., $k_z a << 1$, where $k_z = 2\frac{\pi}{\lambda}$ and a is the cross-section of the filament for the fundamental mode, $\lambda = 2L$), the kink wave speed (v_k) is approximately equal to the phase speed ($v_{\rm ph}$).

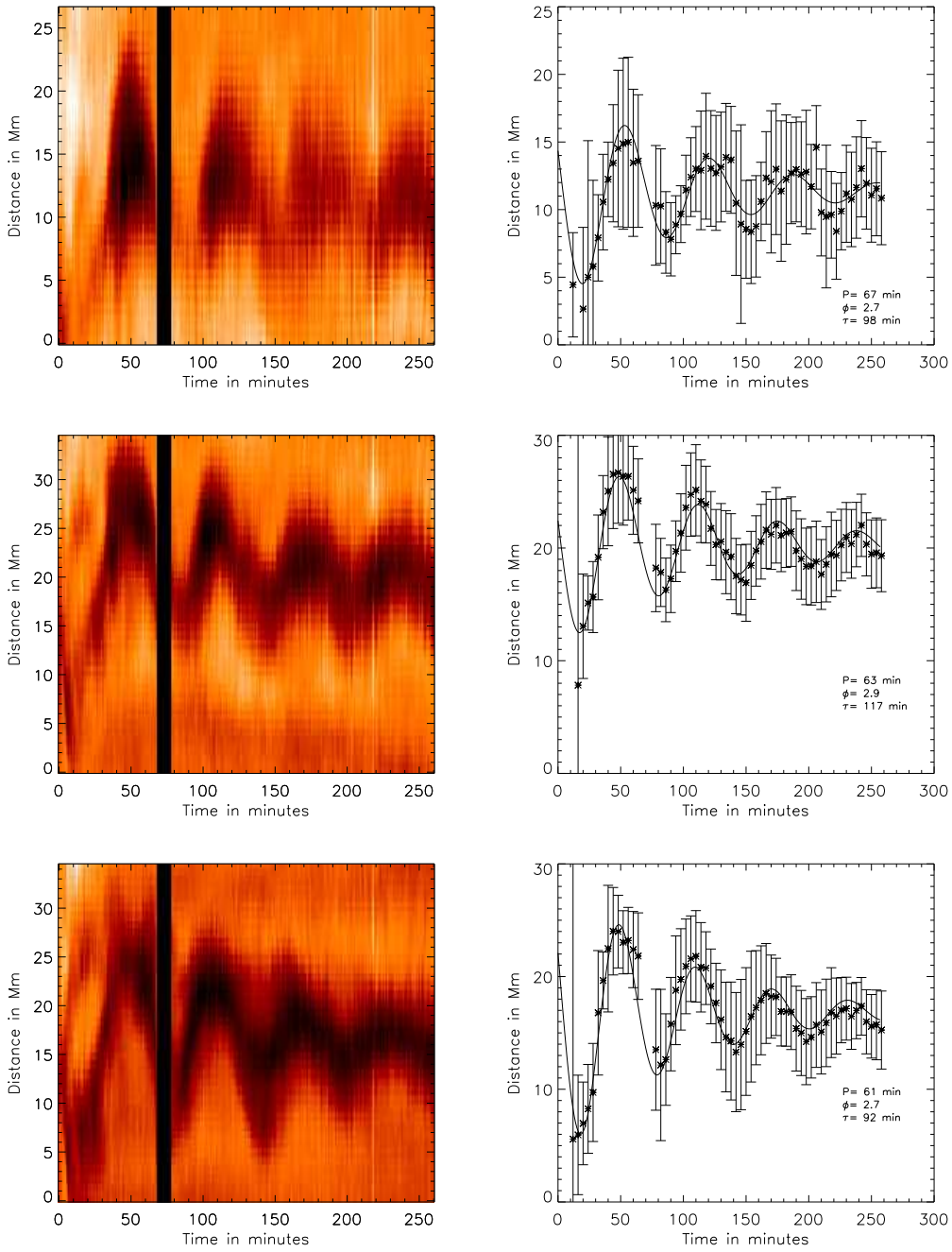

Fig. 2 *Left*: time-distance maps (*top to bottom*) corresponding to the locations of three slices as marked in Fig. 1 by white, yellow and black lines respectively. *Right*: Exponentially damped sinusoidal curves.

An analytical relation between the period of oscillation P, the internal Alfvén travel time $\tau_{\mathrm{A},i}$ and the density ratio ζ is given by

$$y = \frac{\tau_{\mathrm{A},i}}{P} = \frac{1}{\sqrt{2}} \left(\frac{\zeta}{\zeta + 1} \right)^{1/2} , \tag{3}$$

where $\tau_{\mathrm{A},i} = L/v_{\mathrm{A},i}$, the internal Alfvén speed $v_{\mathrm{A},i} = \frac{B}{\sqrt{\mu \rho_i}}$, μ is the permeability of the medium, and ρ_i is the density inside the filament (Goossens et al. 2008). We take $\mu = 4\pi \times 10^{-7}$ H m^{-1} in SI units. ζ in Equation (3) is the internal to external density ratio $\frac{\rho_i}{\rho_e}$. From Equation (3), the Alfvén speed inside the filament tube is given by

$$v_{\mathrm{A},i} = \sqrt{2} \frac{L}{P} \left(\frac{\zeta + 1}{\zeta} \right)^{1/2} . \tag{4}$$

The damping time of the fast kink waves may provide insight into behavior of the ambient plasma and structure of the filament. Arregui et al. (2008) proposed resonant absorption as a damping mechanism in the context of oscillations in prominence fine structure. With the thin boundary (TB) approximation, the analytical expression of the damping time in the asymptotic limit in Cartesian coordinates was derived by Hollweg & Yang (1988) and later by Goossens et al. (1992) and Ruderman & Roberts (2002). The asymptotic expression is (see Goossens et al. 2006; Arregui et al. 2008)

$$\frac{\tau_{\mathrm{d}}}{P} = \frac{2}{\pi} \frac{R}{l} \frac{\rho_i + \rho_e}{\rho_i - \rho_e} , \tag{5}$$

where R is the mean radius of the filament and l is the thickness of its non-uniform layer. Sinusoidal variation of the density is assumed across its non-uniform layer, leading to the factor of $\frac{2}{\pi}$ (Ruderman & Roberts 2002) instead of $\frac{4}{\pi^2}$ for linear variations (Goossens et al. 1992). Using Equation (5), we can express the inhomogeneity length scale ($z = l/2R$) as (Goossens et al. 2008)

$$z = \frac{1}{C} \frac{\zeta + 1}{\zeta - 1} , \tag{6}$$

where C is $\frac{\pi \tau_{\mathrm{d}}}{P}$.

However, the first paper that consistently used information on period and damping time was by Arregui et al. (2007). It used the full numerical results of the eigenvalue computations and its scheme was fully numerical. From Equations (4) and (6), we note that there are three unknown parameters, $v_{\mathrm{A},i}$, ζ and z. There are an infinite number of choices for $v_{\mathrm{A},i}$, ζ and z available that satisfy Equations (4) and (6). Therefore, we have to estimate one unknown and must express the other two unknowns in terms of it. We consider fixing the density ratio (ζ) and express the Alfvén speed ($v_{\mathrm{A,i}}$) and inhomogeneity length scale (z) in terms of ζ.

The maximum value of ζ is infinity. Since z is a decreasing function of ζ, z attains the lowest possible value for the largest possible value of ζ. Thus $z_{\min} = \frac{1}{C}$ for $\zeta \to \infty$. The maximum possible value of z is 1. Therefore, the minimum value of ζ will be when $z = 1$, which can be computed using Equation (6) as $\zeta_{\min} = \frac{C+1}{C-1}$ and using Equation (4) as $v_{\mathrm{A},i,\max} = \frac{2L}{P} \sqrt{\frac{C}{C+1}}$. In the next step, we separately compute the magnetic field strength and inhomogeneity length scale corresponding to slices I (the first), II (the second) and III (the third) for a fixed value of ζ.

4.1 Density Estimates Using Automated DEM Analysis

It is evident that the Alfv́en speed in a medium depends on magnetic field strength and density of the medium. Using Equation (4), Alfv́en speed can be estimated for a given value of ζ. Therefore, the

magnetic field inside the filament can be estimated if density of the filament is known. To estimate density values we follow an automated temperature and emission measurement analysis technique that was developed by Aschwanden et al. (2013) to derive the average density and temperature inside the filament tube. Using this technique, the electron density ($n_{\rm e}$) and temperature (T_e) inside the filament are estimated to be $10^{8.60\pm0.32}$ cm^{-3} and $10^{5.93\pm0.25}$ K respectively (see Fig. 3). Note that the density is underestimated as compared to the typical density range of prominences which extends from 10^9 to 10^{11} cm^{-3} for quiescent and active filaments (Labrosse et al. 2010). We feel that because of the low density ratio with respect to the background that is visible in various *SDO*/AIA channels, the DEM method does not work very well. Furthermore, the observed filament is made-up of mostly cooler material, whereas various AIA channels are sensitive to hotter plasmas, thus the contribution from the prominence material would be minimal. The bright points seen in the AIA 171 Å channel (see Fig. 3) correspond to the prominence-corona transition region (PCTR). Hence, the density values calculated by the DEM technique are the density values of the PCTR associated with this prominence, rather than the bulk of the prominence material. Thus the DEM forward fitting will not be accurate enough for the prominence. By DEM analysis we wish to estimate the PCTR magnetic field. If we use these density estimates (from DEM) and assuming the number density ratio H:He to be 10:1 inside the filament, values of the magnetic field strength (B) for density ratio $\zeta = 100$ are estimated as 0.86$\pm$0.21 G (0.91$\pm$0.20 G and 0.94$\pm$0.20 G) for the first (second and third) slice respectively. These magnetic field strengths are much lower than those reported in Mackay et al. (2010) for the quiescent filaments (3–15 G), which implies that the magnetic field of the overlying PCTR is less than the typical magnetic field of a filament.

4.2 Estimation of the Magnetic Field and Inhomogeneity Length Corresponding to Slice I

Since automated DEM analysis underestimates the density values, we take typical density values in the filament channel which range from 10^9 to 10^{11} cm^{-3}. Using the observed period of $P = 67 \pm 2$ min as well as the damping time $\tau_{\rm d} = 98 \pm 47$ min, we get $\frac{\tau_{\rm d}}{P} = 1.46 \pm 0.76$. For simplicity, henceforth in the paper we consider the absolute values of the parameters without error bars. For example, we derive the extreme values of the seismic quantities as $C = 4.59$, $\zeta_{\rm min} = 1.557$, $z_{\rm min} = 0.218$ and $v_{{\rm A},i,{\rm max}} = 106$ km s^{-1}. Table 1 shows the value of $v_{{\rm A},i}$ and z for different values of ζ. There are an infinite number of choices as shown in Table 1, but we take a typical value of ζ for the filament to be 100. For $\zeta = 100$, the Alfvén velocity and $z = \frac{l}{2R}$ are 83.08 km s^{-1} and 0.222, respectively, thus $l/R = 0.444$. For typical density values in the filament channel (10^9 to 10^{11} cm^{-3}), we deduce the magnetic field value to be ∼1.36 G, ∼4.28 G and ∼13.6 G, respectively.

4.3 Estimation of the Magnetic Field and Inhomogeneity Length Corresponding to Slice II

Using the observed period $P = 63 \pm 2$ min and damping time scale $\tau_{\rm d} = 117 \pm 45$ min, we get $\frac{\tau_{\rm d}}{P} = 1.86 \pm 0.77$. The seismic quantities C, $\zeta_{\rm min}$, $z_{\rm min}$ and $v_{{\rm A},i,{\rm max}}$ are calculated as 5.83, 1.414, 0.171, and 115 km s^{-1}, respectively. For $\zeta = 100$, the Alfvén velocity and $z = \frac{l}{2R}$ are 88.36 km s^{-1} and 0.175, respectively, thus $l/R = 0.350$. Assuming similar density values as those for slice I, i.e., $n_{\rm e} = 10^9$, 10^{10} and 10^{11} cm^{-3}, the magnetic field strength B for the given density ratio $\zeta = 100$ is estimated to be ∼1.44 G, ∼4.56 G and ∼14.46 G, respectively.

4.4 Estimation of the Magnetic Field and Inhomogeneity Length Corresponding to Slice III

Using the observed period $P = 61 \pm 2$ min and damping time $\tau_{\rm d} = 92 \pm 28$ min, we get $\frac{\tau_{\rm d}}{P} = 1.51 \pm 0.51$. The seismic quantities C, $\zeta_{\rm min}$, $z_{\rm min}$ and $v_{{\rm A},i,{\rm max}}$ are calculated as 4.74, 1.534, 0.211, and 116.69 km s^{-1}, respectively. For $\zeta = 100$, the Alfvén velocity and $z = \frac{l}{2R}$ are 91.26 km s^{-1} and 0.215, respectively, thus $l/R = 0.430$. Assuming similar densities as those for slice I, i.e., $n_{\rm e} = 10^9$,

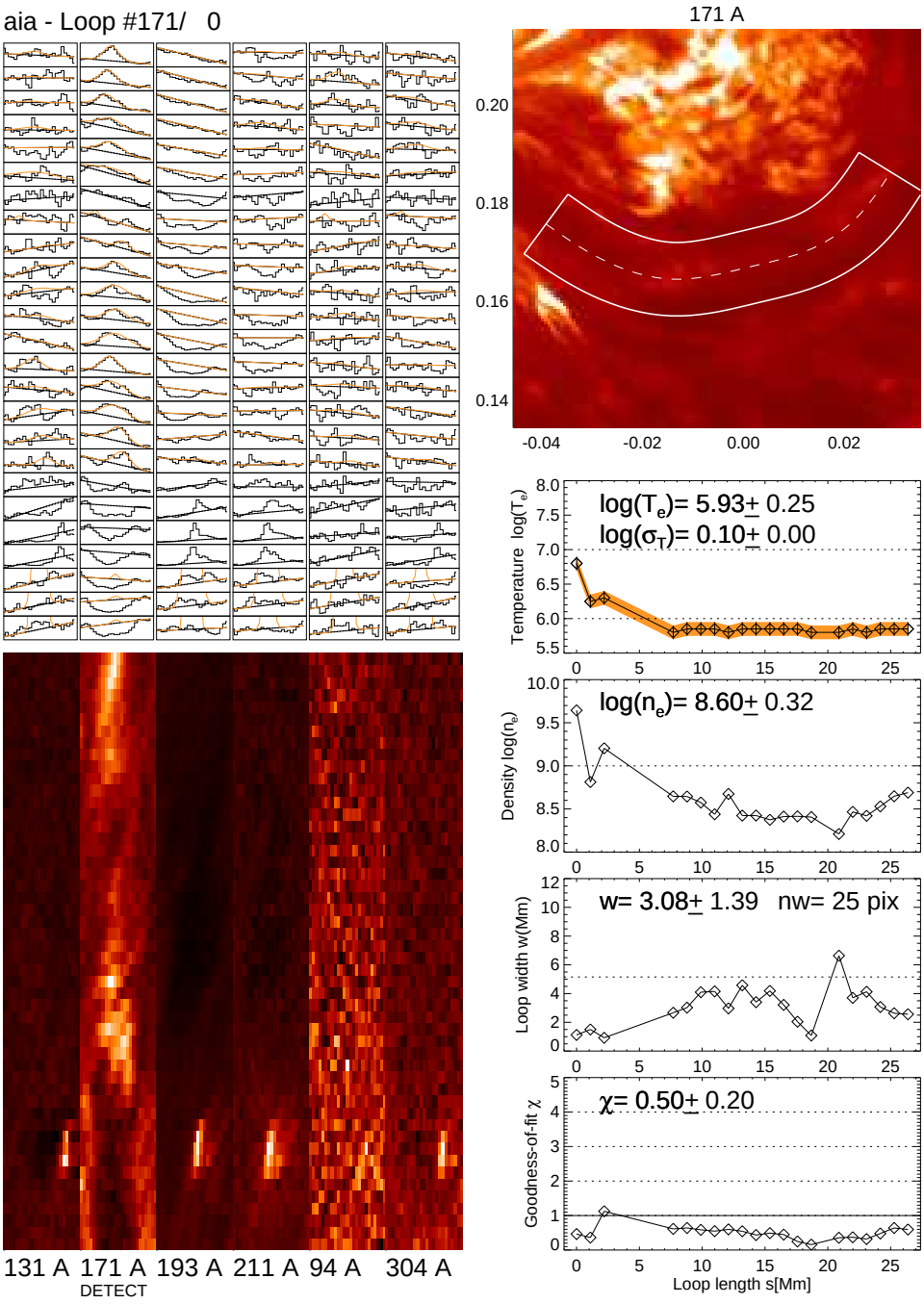

Fig. 3 Automated DEM analysis measurements: (i) the selected segment of the tube (*top-right*) which is also shown in various channels of the AIA (*bottom-left*). (ii) The forward DEM fitting over the emission derived along the chosen path (*top-left*), and derived density as well as temperature (corresponding blocks are shown in the bottom-right multipanel plot).

Table 1 Seismic Parameters related to Exponential Damping

	Slice I		Slice II		Slice III	
ζ	$v_{\mathrm{A},i}$	z	$v_{\mathrm{A},i}$	z	$v_{\mathrm{A},i}$	z
1.414	–	–	115	1	–	–
1.534	–	–	113	0.814	116.69	1
1.557	106	1	112.67	0.787	116.37	0.968
2	101.25	0.654	107.68	0.515	111.21	0.633
3	95.46	0.436	101.52	0.343	104.85	0.422
4	92.42	0.363	98.30	0.286	101.52	0.352
5	90.56	0.327	96.31	0.257	99.47	0.316
6	89.29	0.305	94.97	0.240	98.07	0.295
7	88.38	0.290	94	0.229	97.07	0.281
8	87.69	0.280	93.25	0.220	96.31	0.271
9	87.14	0.272	92.68	0.214	95.72	0.264
10	86.71	0.266	92.21	0.210	95.24	0.258
50	83.49	0.227	88.79	0.179	91.71	0.220
100	83.08	0.222	88.36	0.175	91.26	0.215
1000	82.71	0.218	87.97	0.172	90.85	0.211
.	.	.	.	.	.	.
.	.	.	.	.	.	.
∞	82.67	0.218	87.92	0.171	90.80	0.211

10^{10} and 10^{11} cm^{-3}, the magnetic field strength B for the given density ratio $\zeta = 100$ is estimated to be $\sim$1.48 G, $\sim$4.70 G and $\sim$14.85 G, respectively.

4.5 Estimation of the Magnetic Field and Inhomogeneity Length for Infinite Density Ratio

Seismology is performed by using both P and τ_D and the two coupled equations (Eqs. (4)–(6)). We keep the one unknown, i.e. density ratio, fixed and express the Alfvén speed and inhomogeneity length scale in terms of it. In the case of prominence plasmas, if we consider that the density ratio is large and tending towards infinity, we get two uncoupled equations in which one is related to the period and Alfvén speed, while the other is related to the damping ratio with the inhomogeneity length scale (l/R). Therefore, the inversion that we performed earlier is independent of the density ratio. This is clearly evident from Table 1 which shows that various parameters have very similar values for higher values of ζ (=1000, ∞). For $\zeta = \infty$ for slices I, II and III, the Alfvén velocities and $z = \frac{l}{2R}$ are (82.67, 87.92, 90.8) km s^{-1} and (0.218, 0.171, 0.211), respectively, thus $l/R = (0.436, 0.342, 0.422)$. The magnetic field strength estimated for $\zeta = \infty$ is similar to what is estimated by assuming $\zeta = 100$ in the first decimal place.

5 SUMMARY AND DISCUSSION

A dynamical study of the cool filament observed on-disk in Hα has been performed. We report global kink oscillations in the filament system as observed in Hα as the whole filament tube oscillates in the transverse mode. The oscillation is most likely excited by large scale disturbances originating from a nearby M1.1-class flare. However, we do not aim to understand the nature of the driver or information about its properties, because these topics are outside the scope of our present article. Time series analysis revealed a period between 61 to 67 min and a damping time between 92 to 117 min associated with the kink oscillations around the apex of the filament system. The phase speed (v_{ph}) is found to be between $\sim$117 km s^{-1} and 128 km s^{-1}. These are long-period damped fast kink oscillations, as the phase speed is high compared to the chromospheric sound speed. We also find that oscillations are damped. Lin et al. (2009) have analyzed prominence seismology in prominence

threads and estimated a magnetic field of about 0.1–20 G. However, we have also analyzed the associated seismology in a consistent way using the values of the periods and the damping times at the same time. It is worthwhile emphasizing the application of seismology using the values of the periods and the damping times as it gives an order of magnitude for an estimate of the Alfvén speed inside the prominence (Goossens et al. 2008) and hence on the estimation of the magnetic field strength. Pintér et al. (2008) carried out prominence seismology and calculated the axial component of the magnetic field in a polar crown prominence to be 1–5 G. They used a twisted flux rope model to calculate the magnetic field values. To the best of our knowledge, there have not been any reports yet on consistent seismology in large amplitude oscillations of the prominence, which we implement in the present work to diagnose the local plasma conditions of the observed filament tube. The main result from this study is the estimation of the inhomogeneity length scale. Assuming a typical density ratio ζ of the filament to be 100, the inhomogeneity length scale l/R is 0.444 (0.350 and 0.430) for the first (second and third) slice, respectively, which suggests that the inhomogeneous layer is quite thick near the apex of the filament. An estimate of the density ratio is not very accurate, since there are an infinite number of choices, so from the available information we can say that $l/R > 0.436$ (0.342 and 0.422) for the first (second and third) slice, respectively. We find the magnetic field strength, using the typical density values in the filament, to be in the range of $\sim$1 G to 15 G, which is close to what has been reported by Lin et al. (2009) for the prominence threads. To the best of our knowledge, this is the first time an inhomogeneity length scale and magnetic field strength of a filament as a whole have been estimated using the period of oscillation and damping time simultaneously. Ruderman & Terradas (2013) reported that the amplitude decay in standing kink oscillations for sufficiently small time is described by a Gaussian function and becomes exponential for a later time. The transition from Gaussian to exponential depends on the inhomogeneity length scale. Similar studies have been carried out by Pascoe et al. (2012) and Hood et al. (2013) for propagating waves. Since knowledge of the inhomogeneity length scale is not known *a priori*, we use a Gaussian profile to investigate how it affects the seismology parameters. We find that Alfv́en speed and magnetic field strength are almost the same as calculated using exponential damping. However, inhomogeneity length scale is different because the Gaussian function falls more slowly than the exponential function and therefore damping time is large. Therefore, we conjecture, based on our MHD seismology, that the inhomogeneous layer was already present when the global kink oscillations were excited. This further causes the quick damping of the oscillations via resonant absorption through the well evolved inhomogeneous layer across the prominence tube.

Acknowledgements We would like to thank the referee for his/her valuable comments which enabled us to improve the manuscript. M.G. acknowledges support from KU Leuven via GOA/2009-009 and also partial support from the Interuniversity Attraction Poles Programme initiated by the Belgian Science Policy Office (IAP P7/08 Charm). PFC is supported by the Chinese foundations 2011CB811402 and the National Natural Science Foundation of China (Grant Nos. 11025314, 10933003 and 10673004).

References

Andries, J., Arregui, I., & Goossens, M. 2005, ApJ, 624, L57
Andries, J., van Doorsselaere, T., Roberts, B., et al. 2009, Space Sci. Rev., 149, 3
Arregui, I., Andries, J., Van Doorsselaere, T., Goossens, M., & Poedts, S. 2007, A&A, 463, 333
Arregui, I., & Ballester, J. L. 2011, Space Sci. Rev., 158, 169
Arregui, I., Terradas, J., Oliver, R., & Ballester, J. L. 2008, ApJ, 682, L141
Arregui, I., Oliver, R., & Ballester, J. L. 2012, Living Reviews in Solar Physics, 9, 2
Aschwanden, M. J., Fletcher, L., Schrijver, C. J., & Alexander, D. 1999, ApJ, 520, 880
Aschwanden, M. J., Boerner, P., Schrijver, C. J., & Malanushenko, A. 2013, Sol. Phys., 283, 5

Chen, P. F., Innes, D. E., & Solanki, S. K. 2008, A&A, 484, 487
Edwin, P. M., & Roberts, B. 1983, Sol. Phys., 88, 179
Erdélyi, R., & Taroyan, Y. 2008, A&A, 489, L49
Eto, S., Isobe, H., Narukage, N., et al. 2002, PASJ, 54, 481
Gilbert, H. R., Daou, A. G., Young, D., Tripathi, D., & Alexander, D. 2008, ApJ, 685, 629
Goossens, M., Hollweg, J. V., & Sakurai, T. 1992, Sol. Phys., 138, 233
Goossens, M., de Groof, A., & Andries, J. 2002, in ESA Special Publication, 505, SOLMAG 2002, Proceedings of the Magnetic Coupling of the Solar Atmosphere Euroconference, ed. H. Sawaya-Lacoste, 137
Goossens, M., Andries, J., & Arregui, I. 2006, Royal Society of London Philosophical Transactions Series A, 364, 433
Goossens, M. 2008, in IAU Symposium 247, eds. R. Erdélyi, & C. A. Mendoza-Briceno, 228
Goossens, M., Arregui, I., Ballester, J. L., & Wang, T. J. 2008, A&A, 484, 851
Goossens, M., Terradas, J., Andries, J., Arregui, I., & Ballester, J. L. 2009, A&A, 503, 213
Goossens, M., Van Doorsselaere, T., Soler, R., & Verth, G. 2013, ApJ, 768, 191
Hershaw, J., Foullon, C., Nakariakov, V. M., & Verwichte, E. 2011, A&A, 531, A53
Hollweg, J. V., & Yang, G. 1988, J. Geophys. Res., 93, 5423
Hood, A. W., Ruderman, M., Pascoe, D. J., et al. 2013, A&A, 551, A39
Isobe, H., & Tripathi, D. 2006, A&A, 449, L17
Jing, J., Lee, J., Spirock, T. J., et al. 2003, ApJ, 584, L103
Jing, J., Lee, J., Spirock, T. J., & Wang, H. 2006, Sol. Phys., 236, 97
Labrosse, N., Heinzel, P., Vial, J.-C., et al. 2010, Space Sci. Rev., 151, 243
Lemen, J. R., Title, A. M., Akin, D. J., et al. 2012, Sol. Phys., 275, 17
Li, T., & Zhang, J. 2012, ApJ, 760, L10
Lin, Y., Engvold, O. R., & Wiik, J. E. 2003, Sol. Phys., 216, 109
Lin, Y., Engvold, O., Rouppe van der Voort, L., Wiik, J. E., & Berger, T. E. 2005, Sol. Phys., 226, 239
Lin, Y., Soler, R., Engvold, O., et al. 2009, ApJ, 704, 870
Liu, R., Liu, C., Xu, Y., et al. 2013, ApJ, 773, 166
Luna, M., Díaz, A. J., & Karpen, J. 2012, ApJ, 757, 98
Luna, M., & Karpen, J. 2012, ApJ, 750, L1
Luna, M., Knizhnik, K., Muglach, K., et al. 2014, ApJ, 785, 79
Mackay, D. H., Karpen, J. T., Ballester, J. L., Schmieder, B., & Aulanier, G. 2010, Space Sci. Rev., 151, 333
Markwardt, C. B. 2009, in Astronomical Society of the Pacific Conference Series, 411, Astronomical Data Analysis Software and Systems XVIII, eds. D. A. Bohlender, D. Durand, & P. Dowler, 251
Nakariakov, V. M., Ofman, L., Deluca, E. E., Roberts, B., & Davila, J. M. 1999, Science, 285, 862
Nakariakov, V. M., & Verwichte, E. 2005, Living Reviews in Solar Physics, 2, 3
Ning, Z., Cao, W., Okamoto, T. J., Ichimoto, K., & Qu, Z. Q. 2009, A&A, 499, 595
Ofman, L., & Wang, T. 2002, ApJ, 580, L85
Okamoto, T. J., Nakai, H., Keiyama, A., et al. 2004, ApJ, 608, 1124
Okamoto, T. J., Tsuneta, S., Berger, T. E., et al. 2007, Science, 318, 1577
Oliver, R., & Ballester, J. L. 2002, Sol. Phys., 206, 45
Pascoe, D. J., Hood, A. W., de Moortel, I., & Wright, A. N. 2012, A&A, 539, A37
Pintér, B., Jain, R., Tripathi, D., & Isobe, H. 2008, ApJ, 680, 1560
Ramsey, H. E., & Smith, S. F. 1966, AJ, 71, 197
Roberts, B., Edwin, P. M., & Benz, A. O. 1984, ApJ, 279, 857
Ruderman, M. S., & Erdélyi, R. 2009, Space Sci. Rev., 149, 199
Ruderman, M. S., & Roberts, B. 2002, ApJ, 577, 475
Ruderman, M. S., & Terradas, J. 2013, A&A, 555, A27
Schmieder, B., Kucera, T. A., Knizhnik, K., et al. 2013, ApJ, 777, 108

Soler, R., Goossens, M., Terradas, J., & Oliver, R. 2013, ApJ, 777, 158
Srivastava, A. K., Dwivedi, B. N., & Kumar, M. 2013, Ap&SS, 345, 25
Terradas, J., Molowny-Horas, R., Wiehr, E., et al. 2002, A&A, 393, 637
Terradas, J., Arregui, I., Oliver, R., & Ballester, J. L. 2008, ApJ, 678, L153
Tripathi, D., Isobe, H., & Jain, R. 2009, Space Sci. Rev., 149, 283
Van Doorsselaere, T., Nakariakov, V. M., & Verwichte, E. 2008, ApJ, 676, L73
Vršnak, B., Veronig, A. M., Thalmann, J. K., & Žic, T. 2007, A&A, 471, 295
Yi, Z., & Engvold, O. 1991, Sol. Phys., 134, 275
Yi, Z., Engvold, O., & Keil, S. L. 1991, Sol. Phys., 132, 63
Zhang, Q. M., Chen, P. F., Xia, C., & Keppens, R. 2012, A&A, 542, A52